Chemical Engineering Journal 335 (2018) 560–566

Contents lists available at ScienceDirect

Chemical Engineering Journal

journal homepage: www.elsevier.com/locate/cej

Fabrication of porous SnSeS nanosheets with controlled porosity and their enhanced thermoelectric performance

Hyun Ju, Kiho Kim, Dabin Park, Jooheon Kim*

School of Chemical Engineering & Materials Science, Chung-Ang University, Seoul 06974, Republic of Korea

GRAPHICAL ABSTRACT

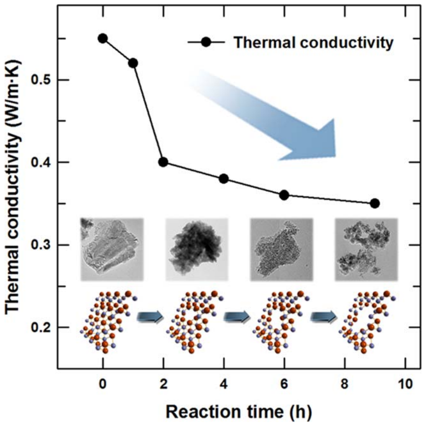

ARTICLE INFO

Keywords:
Thermoelectrics
Chalcogenides
Nanosheets
Porous materials

ABSTRACT

IV–VI-group Sn–chalcogenide-based nanomaterials have attracted interest in various research fields because they offer unique characteristics distinct from their bulk counterparts. The introduction of pores can manipulate the electrical and thermal transport characteristics of the material, which is considered a promising strategy to improve the thermoelectric properties. Herein, we report on the successful fabrication and optimization of porous SnSeS-based nanosheets and their thermoelectric enhancement. Two-dimensional $SnSe_{0.8}S_{0.2}$ (SnSeS) nanocrystals are chemically exfoliated from a layered bulk structure through a Li-intercalation and exfoliation process. Many pores are successfully introduced to the SnSeS nanosheets by solution-phase chemical transformation, and the porosity of the materials is optimized by manipulating the reaction time, resulting in the effective reduction of the thermal conductivity and enhancement of the thermoelectric performance. The incorporation of nanoscale and porous structure can accelerate research advances regarding nanoscale porous materials and high-performance thermoelectrics.

1. Introduction

Energy harvesting is expected to become an increasingly important technology in overcoming future energy crises. Thermoelectric energy conversion is highly attractive as a promising strategy for energy harvesting because it can be used for devices, directly enabling the generation of electrical energy from temperature gradients [1–4]. The figure of merit (*ZT*) is used to express the thermoelectric performance of

---

* Corresponding author.
E-mail address: jooheonkim@cau.ac.kr (J. Kim).

http://dx.doi.org/10.1016/j.cej.2017.11.003
Received 3 August 2017; Received in revised form 16 October 2017; Accepted 1 November 2017

a material. Low thermal conductivity (κ) is intensely required to achieve a high *ZT*, which is calculated as $ZT = (S^2 \cdot T)/\kappa \cdot \rho$, where *S* is the Seebeck coefficient, *T* is the absolute temperature, and ρ is the electrical resistivity. Previous research has mainly focused on enhancing *ZT* in efficient inorganic materials through the nanostructuring of bulk materials, which contributes to the achievement of lower thermal conductivity, leading to higher *ZT* [5–8]. Nanostructures introduce many boundaries to the bulk material that act as effective phonon scattering positions, thereby increasing the lattice scattering of phonons.

Recently, it has been reported that SnSe has strong potential as an efficient thermoelectric material because it has an extremely low κ value, originating from the strong anharmonicity of its chemical bonds [9–12]. In addition, many experiments regarding the enhancement of *ZT* in SnSe [13–15] and analogous chalcogenides have been reported [16–19]. However, studies on the nanostructuring of SnSe-based materials to achieve significant reductions in the κ value are rare. Another powerful strategy to reduce the κ value is the introduction of nanoscale pores in the structure. The presence of pores in materials can achieve dramatically low κ values, arising from phonon scattering at the porous boundaries, and thereby further improve the *ZT* of the materials. Tang et al. prepared porous Si as an efficient thermoelectric material that exhibited an low κ and outstanding *ZT* value [20]. Zhang et al. fabricated a mesoporous Bi_2Te_3 monolith and reported that the mesoporous Bi_2Te_3 showed an extremely low κ with high *ZT* [21]. Chen et al. achieved a significant reduction in the κ of the cold-pressed higher manganese silicide at 300 K, which could be attributed to the high porosity [22].

Herein, we report on the preparation and optimization of porous $SnSe_{0.8}S_{0.2}$ (SnSeS) nanosheets by the incorporation of nanostructured SnSeS and the introduction of pores to the nanostructure, and the thermoelectric application of the resulting material. Ternary SnSeS crystals have lower κ values than the original SnSe because the substitution of isoelectric S atoms in SnSe causes atomic disorder that generates phonon-scattering positions [23–25]. SnSe-based materials have van der Waals-bonded layered structures along the *a* axis with strong two-atom-thick bonds along the *b*-*c* planes [9,26]; therefore, two-dimensional SnSeS nanostructures can be obtained through an exfoliation procedure from bulk SnSeS. Nano-sized pores are introduced to the prepared nanostructures *via* an organic acid-assisted chemical transformation reaction. We expect that the combination of nanoscale and porous structures can achieve a highly efficient thermoelectric material with an improved *ZT*. In addition, the fabrication procedure could be applied to other porous nanomaterials in various research fields.

2. Experimental section

2.1. Preparation of porous SnSeS nanosheets

Stoichiometric amounts of Sn (99.999%), Se (99.999%), and S (99.999%) corresponding to the composition of $SnSe_{0.8}S_{0.2}$ (SnSeS) were loaded into a quartz ampoule which was evacuated and subsequently sealed by a flame. The ampoule was slowly heated to 1223 K in 10 h, and after holding this temperature for 6 h, the furnace was cooled to 298 K. The prepared SnSeS ingot was ground into fine powder, and 0.5 g of SnSeS powder with a solution containing both 100 mL of ethylene glycol and 0.4 g LiOH was added to a Teflon-lined autoclave. The autoclave was then heated to 473 K for 48 h to intercalate Li^+ ions in the layers of SnSeS. After intercalation, the solution was cooled naturally to 298 K. The resulting product was filtered and washed several times with acetone to eliminate any residual reactants, and then dried in a vacuum oven at 333 K for 24 h. After the procedure, 0.1 g of lithiated SnSeS powder was placed in a beaker filled with 40 mL of deionized (DI) water. The beaker was sealed and sonicated for 1 h. After the resulting dispersion was centrifuged at 1000 rpm for 30 min, the supernatant was collected. The supernatant was then centrifuged at 8000 rpm for 30 min. The resulting product was purified several times with an aqueous HCl solution (3 vol%). After washing the final product with ethanol several times, SnSeS nanosheets were finally obtained by drying in a vacuum oven. 28.25 mg of the resulting SnSeS nanosheets was added to an aqueous solution containing 225 mg of tartaric acid ($C_4H_6O_6$, t-acid) and 100 mL of DI water. After vigorous stirring, the mixture was then transferred into a Teflon-lined autoclave. The vessel was sealed and heated to 503 K for various reaction times (0, 1, 2, 4, 6, and 9 h) for the optimization of the chemical transformation procedure. The resulting product was collected and washed with water and ethanol, and dried in a vacuum oven overnight. Finally, the product was pressed for 10 min at 823 K under 50 MPa, thereby yielding pelletized samples.

2.2. Characterization

X-ray diffraction (XRD; New D8-Advance/Bruker-AXS) at 40 mA and 40 kV, with Cu Kα radiation (0.154056 nm) and a scan rate of 1°/s for 2θ ranging from 5–70°, was used to characterize the crystal structure of the materials. The binding energy peaks of the materials were investigated with X-ray photoelectron spectroscopy (XPS, Thermo U. K. K-alpha) using a monochromated Al Kα X-ray source (1486.6 eV) and a hemispherical analyzer. The morphology and microstructure of the materials were determined by field-emission scanning electron microscopy (FE-SEM, SIGMA) and field-emission transmission electron microscopy (FE-TEM, JEM-2100F). The elemental mappings of the samples were analyzed by energy-dispersive X-ray spectroscopy (EDS, NORAN system 7, Thermo Scientific). A four-point probe method with disk-shaped compressed pellets was used to measure the electrical conductivity. A homemade device containing a pair of thermocouples and voltmeters was used to measure the Seebeck coefficient, *S*. The thermal conductivity of the composites was calculated from the relation $\kappa = \alpha \cdot \rho_d \cdot C_P$, where α is the thermal diffusivity, C_P is the specific heat, and ρ_d is the bulk density of the material. An LFA 447 Nanoflash (NETZSCH) was used to measure the thermal diffusivity. The specific heat was measured using differential scanning calorimetry (DSC 131 Evo, Setaram Instrumentation). The DSC measurements described the thermal transition behavior of the composites, with the samples heated from −20 to 120 °C at a rate of 10 °C/min in a N_2 atmosphere. Vickers hardness of each sample was measured using a micro-vickers hardness tester (MMT-X7, Clemex) at a load of 4.9 N. Five samples were prepared under each condition to assess the reproducibility of our experiments and investigated in the same in-plane direction to avoid the anisotropy of the samples.

3. Results and discussion

Firstly, the SnSeS nanosheets with the stoichiometric composition of Sn, Se, and S (Sn:Se:S = 1:0.8:0.2) were chemically exfoliated from pulverized SnSeS powders prepared using a solid-state reaction and Li-assisted exfoliation process, similar to the technique in our previous research [27]. Fig. 1a shows the X-ray diffraction (XRD) results of the pulverized SnSe and SnSeS powders and the exfoliated SnSeS nanosheets. The diffraction peaks of the SnSeS powder and nanosheets have the same positions, which are shifted slightly to the right compared to the peaks of SnSe powder, which is caused by the smaller anionic radius of S^{2-} (1.70 Å for S^{2-} and 1.84 Å for Se^{2-}) [28]. Fig. 1b–d shows the high-resolution X-ray photoelectron spectroscopy (XPS) spectra of the Sn 3*d*, Se 3*d*, and S 2*p* binding energies of SnSeS, respectively, from the wide-range XPS spectrum of the resulting SnSeS nanosheets (Fig. S1). The peaks at ~494.4 and 485.9 eV in the Sn 3*d* orbital correspond to the Sn $3d_{3/2}$ and Sn $3d_{5/2}$ binding energies, while the Se $3d_{3/2}$ and Se $3d_{5/2}$ peaks are shown at ~54.5 and 53.6 eV. The S 2*p* peak is located at ~161.3 eV. The measured binding energies of the SnSeS are close to those in the previously reported binding energies for Sn^{2+}, Se^{2-}, and S^{2-} [29,30], thereby verifying the successful